remote sensing

MDPI

Article

Hydrological Response Assessment of Land Cover Change in a Peruvian Amazonian Basin Impacted by Deforestation Using the SWAT Model

Karla Paiva [1,*], Pedro Rau [1], Cristian Montesinos [2], Waldo Lavado-Casimiro [2], Luc Bourrel [3] and Frédéric Frappart [4]

[1] Centro de Investigación y Tecnología del Agua (CITA), Universidad de Ingeniería y Tecnología (UTEC), Lima 15063, Peru; prau@utec.edu.pe
[2] Servicio Nacional de Meteorología e Hidrología del Perú (SENAMHI), Lima 15072, Peru; cmontesinos@senamhi.gob.pe (C.M.); wlavado@senamhi.gob.pe (W.L.-C.)
[3] UMR 5563 Géosciences Environnement Toulouse (GET), Université de Toulouse, CNRS, IRD, UPS, CNES, OMP, 14 Avenue Edouard Belin, 31400 Toulouse, France; luc.bourrel@ird.fr
[4] Interactions Sol Plante Atmosphère (ISPA), Institut National de Recherche pour l'Agriculture, l'Alimentation et l'Environnement (INRAE), Bordeaux Sciences Agro, F-33140 Villenave d'Ornon, France; frederic.frappart@inrae.fr
* Correspondence: karla.paiva@utec.edu.pe

Abstract: The watershed hydrologic conditions in the Madre de Dios (MDD) Basin in the Peruvian Amazon have been irreversibly impacted by deforestation and changes in land cover. These changes have also had detrimental effects on the geomorphology, water quality, and aquatic habitat within the basin. However, there is a scarcity of hydrological modeling studies in this area, primarily due to the limited availability of hydrometeorological data. The primary objective of this study was to examine how deforestation impacts the hydrological conditions in the MDD Basin. By implementing the Soil and Water Assessment Tool (SWAT) model, this study determined that replacing 12% of the evergreen broadleaf forest area with bare land resulted in a significant increase in surface runoff, by 38% monthly, a 1% annual reduction of evapotranspiration, and an average monthly streamflow increase of 12%. Changes in spatial patterns reveal that the primary impacted watershed is the Inambari River subbasin, a significant tributary of the Madre de Dios River. This area experiences an annual average surge of 187% in surface runoff generation while witnessing an annual average reduction of 8% in evapotranspiration. These findings have important implications, as they can contribute to instances of flooding and extreme inundation events, which have already occurred in the MDD region.

Keywords: SWAT model; surface runoff; deforestation; land use change; Amazonia; Peru

Citation: Paiva, K.; Rau, P.; Montesinos, C.; Lavado-Casimiro, W.; Bourrel, L.; Frappart, F. Hydrological Response Assessment of Land Cover Change in a Peruvian Amazonian Basin Impacted by Deforestation Using the SWAT Model. *Remote Sens.* **2023**, *15*, 5774. https://doi.org/10.3390/rs15245774

Academic Editor: Gabriel Senay

Received: 12 September 2023
Revised: 10 November 2023
Accepted: 10 December 2023
Published: 18 December 2023

1. Introduction

Madre de Dios (MDD) is an important rainforest region located in the southeastern Peruvian Amazonian and is recognized for its biological and cultural diversity [1–3], with an important biomass stock [4]. Over the last 40 years, this region has been threatened by illegal alluvial gold mining. This activity involves deforestation, soil excavation, and the use of liquid mercury [5], causing permanent loss of the ecosystem, severe soil erosion, water pollution, mercury in hydrobiology, and human health problems [6–10]. Between 1984 and 2017, 100,000 ha of accumulated deforestation due to alluvial gold mining activities was identified [11]. Deforestation increases soil erosion and surface runoff rates, leading to increased sedimentation rates and alteration of the hydrological cycle [12]; removing vegetation cover also increases soil compaction and reduces infiltration capacities, leading to floods [13], which are frequent during the wet seasons, especially in the mining zones of the MDD Basin.

The Soil and Water Assessment Tool (SWAT) is a watershed-scale model widely used to determine hydrologic responses resulting from changes in land use and land cover (LULC) [14]. The SWAT model has been successfully implemented in multiple geographical regions worldwide, to understand how alterations in land use and land cover can influence local hydrology and sediment yields. Significant findings from these studies in the Brazilian Amazonia include the observation of increasing trends in surface runoff and sediment yield, with a simultaneous decrease in evapotranspiration [15]. Additionally, these studies have revealed increased flow during the high-flow season and decreased flow during the low-flow season, leading to the intensification of extreme flow events [16]. The impact of alterations in land use and land cover on hydrology and sediment yields may not be uniform across different geographical regions; uppermost reaches of forested highlands were most significantly affected in an East African Watershed [17], while the change in land use from forest to bare soil would increase the runoff-generating capacity in the Brazilian Amazon much more than if it was replaced by crop or pasture [15].

Even though many interdisciplinary studies have been conducted to assess the impacts of alluvial gold mining in MDD, there is a knowledge gap where hydrological impacts due to deforestation remain unknown, mainly due to the lack of meteorological and hydrological available data. Precipitation data are an essential input to properly represent hydrological processes in hydrological models [18]. Furthermore, it is considered as the first source of uncertainty [19]. Due to the scarce availability of meteorological data measured in the Amazon Basin, several studies have used satellite precipitation data, such as TRMM (Tropical Rainfall Measuring Mission) [20], GMP (Global Precipitation Measurement) [21], and CHIRPS (Climate Hazards Group Infrared Precipitation with Stations) [22], as input for hydrological models [23–25].

The main aim of this study is to assess the effects of deforestation due to gold mining on the hydrological response and providing reliable streamflow daily data for main rivers leading to further studies. This study incorporates the CHIRPS product for precipitation [22] and the CPC Global Unified Temperature provided by NOAA (National Oceanic and Atmospheric Administration) for temperature [26]. The specific objective is to analyze the impact on hydrological variables such as streamflow regime and surface runoff on a future deforestation scenario in one of the areas most affected by deforestation and mining watersheds in the Peruvian Amazonia.

This study is, to the best of our knowledge, the first application of the SWAT model within the Madre de Dios River Basin aimed at simulating the hydrological characteristics of this watershed, likely owing to data scarcity in this ungauged basin. The findings from our research carry substantial scientific significance, as they furnish essential streamflow data for water bodies that currently lack any measured information.

Furthermore, this study bridges a critical gap by addressing the need to comprehend hydrologic regimes for interdisciplinary studies. This knowledge is fundamental for enhancing studies to understand the mobilization of mercury [27] and its primary sources and sinks [28]. Furthermore, it contributes to the study of the effects of alluvial gold mining activities on river morphology and sediment transport [29].

2. Materials and Methods

2.1. Study Area

The Madre de Dios (MDD) Basin (Figure 1) is delimited from the Andes Mountains until the outlet point Amaru Mayu located in the Madre de Dios River after the confluence of the Tambopata River. This basin covers a drainage area of 90,750 km^2 (9075 kha), with an elevation ranging between 170 and 6000 m. The majority of the MDD Basin predominantly consists of Southwest Amazon moist forests with a flat topography, characterized by floodplains exhibiting slopes of less than 5%. However, the basin area formed by the Andes Mountains or Peruvian Yungas displays notably steep slopes, with values exceeding 50%; finally, the northwestern area comprises elevated uplands, with slopes measuring less than 20%.

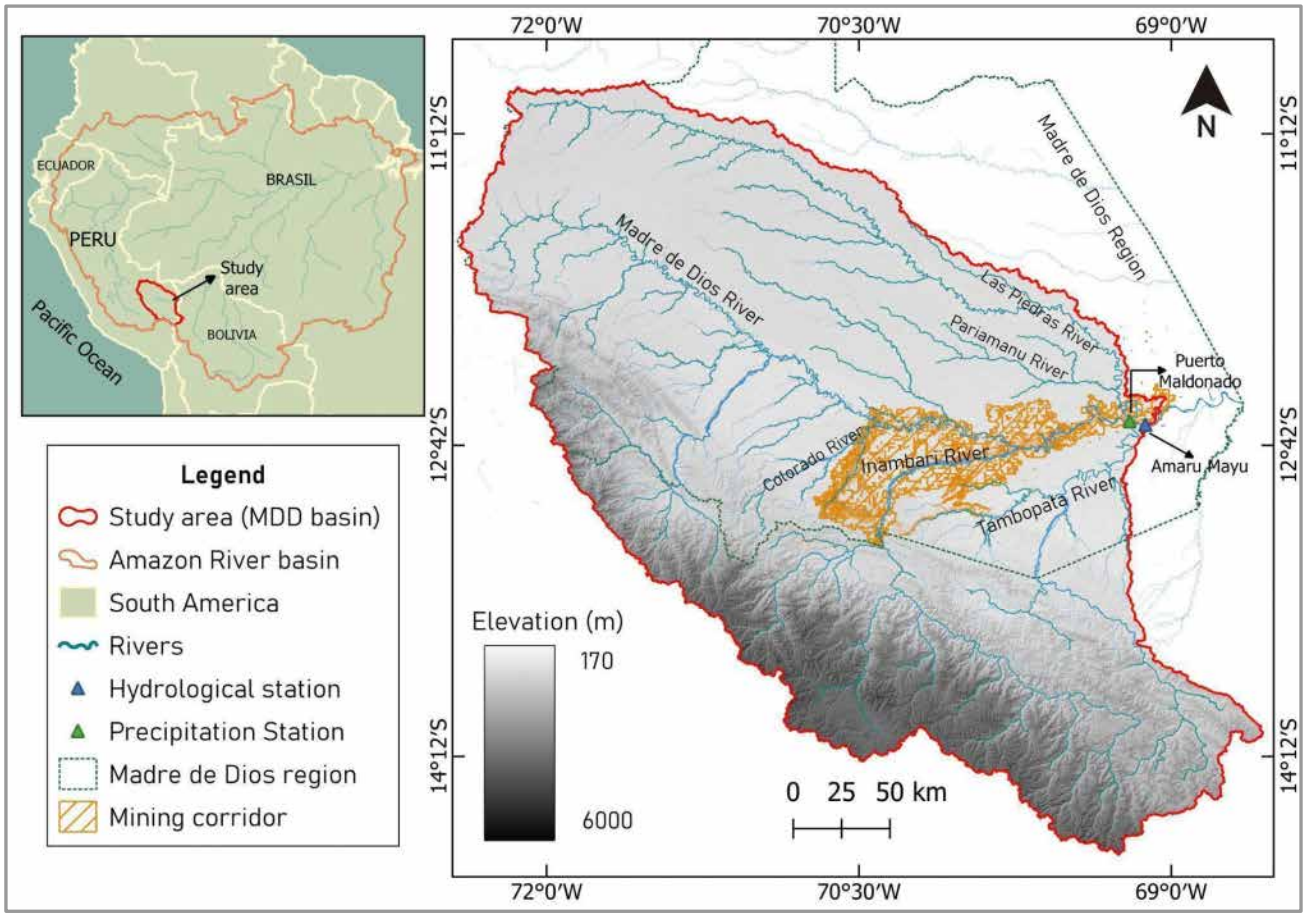

Figure 1. Study area and location map of the meteorological and hydrological stations.

The MDD Basin presents a warm, rainy-to-very-rainy climate (more than 2000 mm/year) throughout the year. The part of the study area bordering the Eastern Cordillera of the Andes is characterized by a highly rainy zone (6000 mm/year, on average) [30]. According to the analysis of the monthly average of measurements from the Puerto Maldonado meteorological station (Figure 1), the maximum precipitation of 384 mm/month occurred in December. The dry months cover the period from May to September, with a minimum precipitation of 32 mm/month in August, and the average precipitation is 2240 mm/year. The average annual minimum and maximum temperatures are 21.9 °C and 31.3 °C, respectively (Figure 2).

Despite the delimited protected areas in the MDD region, this is one of the most severe examples of deforestation caused by gold mining in the entire Amazon [31]. Based on the Global Forest Watch maps of tree cover loss from the Global Land Analysis and Discovery (GLAD) [32], made available by the World Research Institute (WRI), a total area of 2750 km^2 (equivalent to 275 kha) was deforested in the MDD region between 2001 and 2022. Similarly, the Peruvian Ministry of Environment (MINAM) has determined a significant forest loss of 2097 km^2 (209 kha) within the Madre de Dios region between 2001 and 2018 [33].

Even when agriculture concentrates the largest deforestation, mining deforestation has the potential to significantly impact critical areas such as riverbanks, protected areas, and indigenous territories. Deforestation is most intense along the mining corridor (Figure 1); this zone crosses along the Madre de Dios River and its floodplain, including the Colorado and Inambari Rivers.

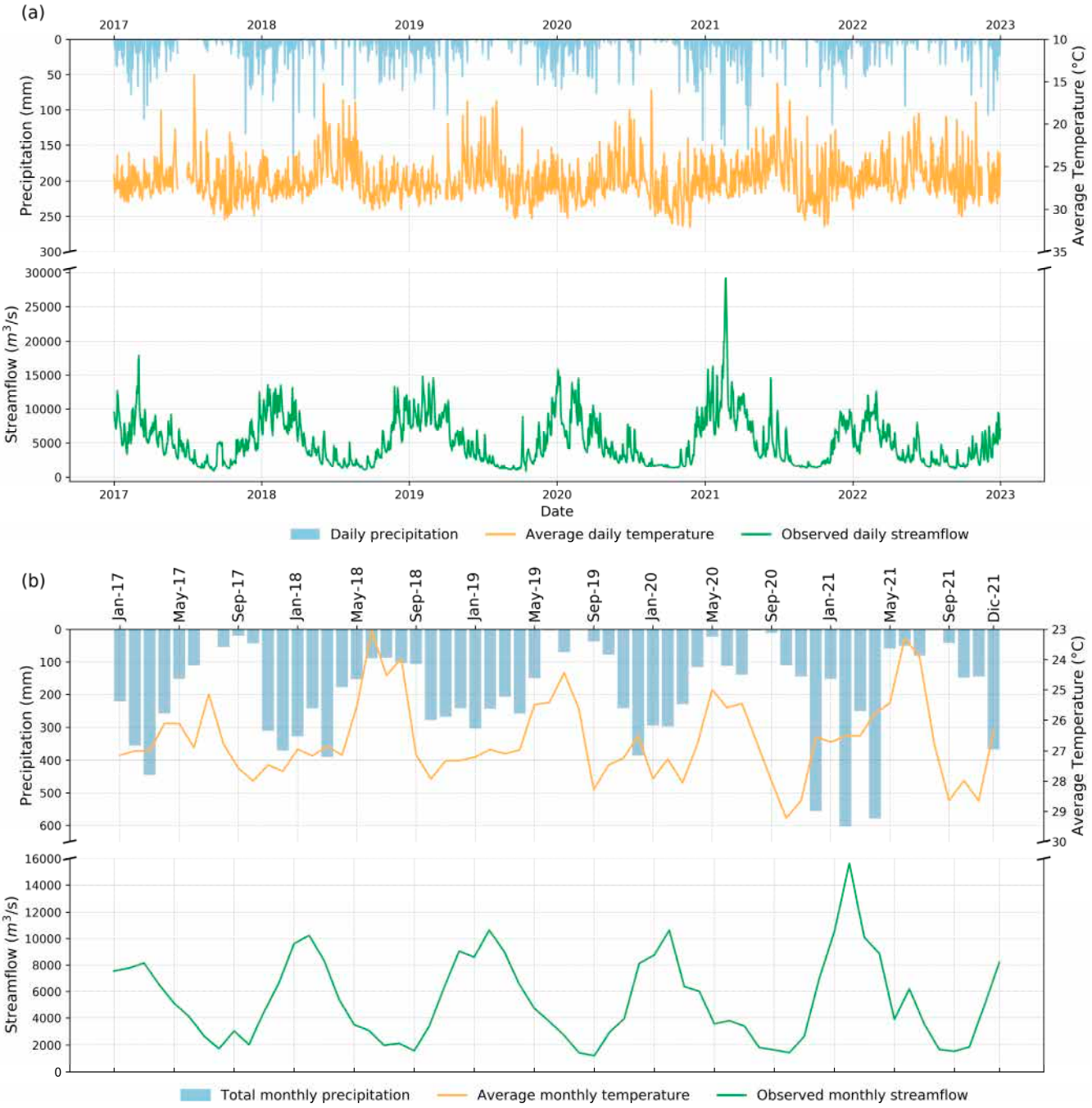

Figure 2. (**a**) Daily and (**b**) accumulated monthly precipitation data, mean temperature plotted on the secondary axis, and observed monthly streamflow at the hydrological station Amaru Mayu (outlet point of the MDD Basin).

2.2. Climate Data

The study area's limited number of precipitation stations led to the evaluation of several gridded datasets. We have assessed the precipitation daily dataset from three gridded products, CHIRPS [22], TRMM [20], and PISCO [34], executing the SWAT model and comparing the resultant streamflow outputs against the observed streamflow measurements obtained from the Amaru Mayu station. For this comparison, we have considered both visual performance analysis and selected the same metrics to evaluate the model's performance [35]. These metrics, which will be defined in the Model setup subsection, are the Nash–Sutcliffe coefficient of efficiency, the percent bias, and the root mean square error.

The dataset demonstrating the highest degree of accuracy was subsequently identified and selected. Daily averaged grids for the period 1981–2021 have been calculated for each subbasin, since SWAT uses the nearest station to the centroid of each subbasin.

Daily maximum and minimum temperature data were obtained from CPC Global Unified Temperature, provided by the NOAA PSL [26]. In this study, 217 and 110 grids were used for precipitation and temperature, respectively, over the period 1995–2021.

Streamflow data were collected from the hydrological station Amaru Mayu, located at the outlet point of the MDD Basin (Figure 1). The data were provided by the National Authority of Water of Peru (Autoridad Nacional del Agua—ANA) [36]. The period available was from 2017 to the present. Average annual streamflow is 5180 $m^3 \cdot s^{-1}$ and the average flow during the dry season (May to September) is 2886 $m^3 \cdot s^{-1}$, while in the wet season (October to April) it is 6819 $m^3 \cdot s^{-1}$, as shown in Figure 2b.

2.3. Topography, Soil, and Land Use Data

The Digital Elevation Model (DEM) utilized in this study originates from the Shuttle Radar Topography Mission (SRTM) and possesses a spatial resolution of 30 m [37]: this information is necessary to delineate the basin, subbasins, and streamflow network. Furthermore, the model requires information about the types of soil and their physical properties, such as texture, water holding capacity, hydraulic conductivity, and others. The soil type map (Figure 3a) was obtained from the Digital Soil Map of the World provided by the Food and Agriculture Organization of the United Nations (FAO) [38]. In the MDD Basin, the soil types are Orthic Acrisols—Medium texture (30%); Lithosol—Dystric Cambisols (18%); Lithosol—Dystric Cambisols–Dystric Regosols (17%); Xanthic Ferralsols (11%); Orthic Acrisols—Heavy texture (8%); Lithosol—Humic Cambisols (6%); Gleyic Acrisols (5%); Dystric Gleysols (3%); and Glacier and Dystric Regosols (less than 1% covering area). The land use cover map used to set up the preliminary SWAT model was from Global Land Cover Characterization (GLCC)—USGS [39]. The map shown in Figure 3b illustrates that the predominant land cover category, comprising 70%, is characterized by evergreen broadleaf forest. Then follows shrubland at a distant proportion of 9%, with grassland occupying 8%, cropland/woodland mosaic encompassing 4%, and savanna and wooded tundra occupying 4% and 3%, respectively, while other categories collectively represent less than 1%. Information related to the datasets presented above are summarized in Table 1.

Table 1. Model input data.

Input Data	Spatial Resolution	Source
Precipitation	0.05° (~5 km)	CHIRPS v2.0 [22]
Temperature	0.5° (~55 km)	CPC Global Unified Temperature [26]
Digital Elevation Model	30 m	SRTM [37]
Soil type map	1:5,000,000	FAO v3.6 [38]
Land use cover map	~0.5 km	GLCC—USGS v2 [39]
Observed streamflow	-	ANA [36]

2.4. SWAT Model

The Soil and Water Assessment Tool (SWAT) is a process-based model designed for continuous-time simulation, featuring a semi-distributed structure. It is particularly suited for the representation of long-term basin-scale processes [40]. SWAT stands out as a versatile and robust tool, capable of simulating diverse watershed scenarios across varying scales and environmental contexts worldwide [41]. The model performs simulations dividing each basin into subbasins. Every subbasin is further subdivided into hydrologic response units (HRUs). Every HRU is a unique combination of land use, soil, and slope in each subbasin; this is why this model is called semi-distributed [42]. In this study, the MDD

Basin was divided into 217 subbasins and a total of 1244 HRUs. The water balance in SWAT is given by Equation (1).

$$SW_t = SW_0 + \sum_{i=1}^{t} \left(R_{day\ i} - Q_{surf\ i} - E_{a\ i} - w_{seep\ i} - Q_{gw\ i} \right) \quad (1)$$

where SW_t is the final soil water content on day t (mm); SW_0 is the initial soil water content on day i (mm); t is time (d); $R_{day\ i}$ is the precipitation depth on day i (mm); $Q_{surf\ i}$ is the surface runoff volume on day i (mm); $E_{a\ i}$ is the evapotranspiration depth on day i (mm); $w_{seep\ i}$ is the amount of water entering the vadose zone from the soil profile on day i; and $Q_{gw\ i}$ is the amount of return flow on day i.

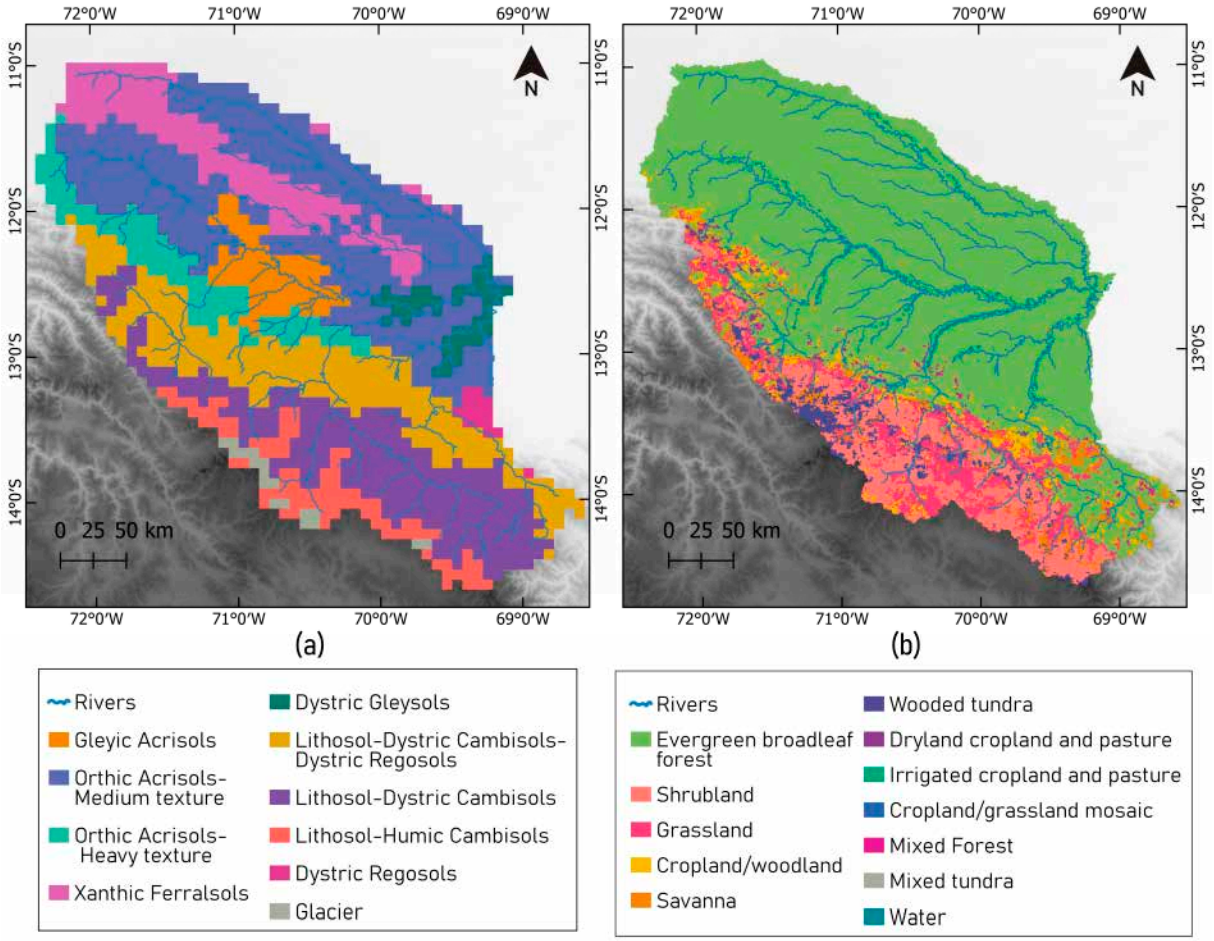

Figure 3. (**a**)Soil type map. Source: Food and Agriculture Organization of the United Nations (FAO). (**b**) Land use cover map. Source: Global Land Cover Characterization (GLCC)—USGS.

2.4.1. Model Setup

In this study, we utilized SWAT version 2012 (SWAT.v.2012) by means of the QSWAT 1.3 plug-in within the open-source Geographic Information System, QuantumGIS (QGIS) [43].

The initial stage of the model, known as the warm-up period, was utilized to enable the hydrological model to operate for a significant duration before the simulation period begins. This allows important processes to reach a state of dynamic equilibrium. To achieve this, model developers suggest implementing warm-up periods lasting two to four years for watershed scale processes [44]. Consequently, in this study, the time period between 1981 and 1984 was utilized as the warm-up period to ensure an appropriate initialization of the system.

The simulation period covered a total period of 32 years, from 1990 to 2022, during which the model executed operational simulations and produced results. The calibration

and validation period, on the other hand, was limited to 2016 to 2020 and 2021 to 2022, respectively, primarily due to data availability. Within this calibration period, the model's parameters were adjusted to achieve the best possible fit with observed streamflow data.

The assessment of the model's performance consisted of a thorough examination, specifically comparing the observed and simulated streamflow data, focusing on subbasin number 215, which corresponds to the Amaru Mayu hydrological station, during the period from 2016 to 2021. The validation process utilized the metrics outlined in Table 2 [45]. These metrics included the Nash–Sutcliffe coefficient of efficiency (NS) [46], calculated using Equation (2), the percent bias (PBIAS) [47] determined through Equation (3), and the root mean square error (RMSE)-observations' standard deviation ratio (RSR) [45], as derived from Equation (4). The coefficient of determination, R^2, was not taken in account since linear model assumptions can suffer significant offset error [35]

$$NSE = 1 - \frac{\sum_{i=1}^{n}(Q_i - {Q_i}^c)^2}{\sum_{i=1}^{n}(Q_i - \underline{Q})^2} \quad (2)$$

$$PBIAS = \frac{\sum_{i=1}^{n}(Q_i - {Q_i}^c)}{\sum_{i=1}^{n}(Q_i)} \times 100\% \quad (3)$$

$$RSR = \frac{RMSE}{STDEV_{obs}} = \frac{\sqrt{\sum_{i=1}^{n}(Q_i - {Q_i}^c)^2}}{\sqrt{\sum_{i=1}^{n}(Q_i - \underline{Q})^2}} \quad (4)$$

where Q_i is the observed streamflow on day i; ${Q_i}^c$ is the simulated streamflow on day i; and $\underline{Q}$ is the mean observed streamflow.

Table 2. Statistics evaluated for the assessment of streamflow performance in a monthly time step [45].

Performance Rating	NS [1]	PBIAS [2]	RSR [3]
Very good	$0.75 \leq$ NS ≤ 1.00	PBIAS $\leq \pm 15\%$	$0 \leq$ RSR ≤ 0.5
acceGood	$0.65 \leq$ NS ≤ 0.75	$\pm 15\% \leq$ PBIAS $\leq \pm 30\%$	$0.5 \leq$ RSR ≤ 0.6
Satisfactory	$0.5 \leq$ NS ≤ 0.65	$\pm$ 30% $\leq$ PBIAS $\leq \pm 55\%$	$0.6 \leq$ RSR ≤ 0.7
Unsatisfactory	NS ≤ 0.5	PBIAS $\geq \pm 55\%$	RSR ≥ 0.7

[1] NS: Nash–Sutcliffe coefficient of efficiency; [2] PBIAS: percent bias; [3] RSR: root mean square error-observations standard deviation ratio.

2.4.2. Deforestation Scenario

The SWAT model provides a database with parameter values for various vegetation types and crops. These parameters represent the physical and physiological properties of the vegetation [42]. The land use map contains the different types and distribution of land cover in each subbasin of the study area, allowing the model to simulate and integrate responses of various cover types, and enabling modelers to study land use cover change impacts by varying the spatial and temporal distributions [48].

The "National Forest Conservation Program for Climate Change Mitigation" is under the management of the Peruvian Ministry of Environment (MINAM) and, using data from the Landsat 7 and 8 satellites, MINAM has established a methodology to identify early warning alerts for the loss of humid tropical forest cover in Peru. These alerts, which are accessible via the Geobosques platform http://geobosques.minam.gob.pe (accessed on 20 March 2023), show that among Peruvian regions, Madre de Dios consistently registers the highest density of these alerts annually, surpassing other areas [49]. Figure 4 shows deforestation national alerts density (black color in the right enlarged image) inside the mining corridor and even inside the buffer zone of the National Tambopata Reserve (blue color).

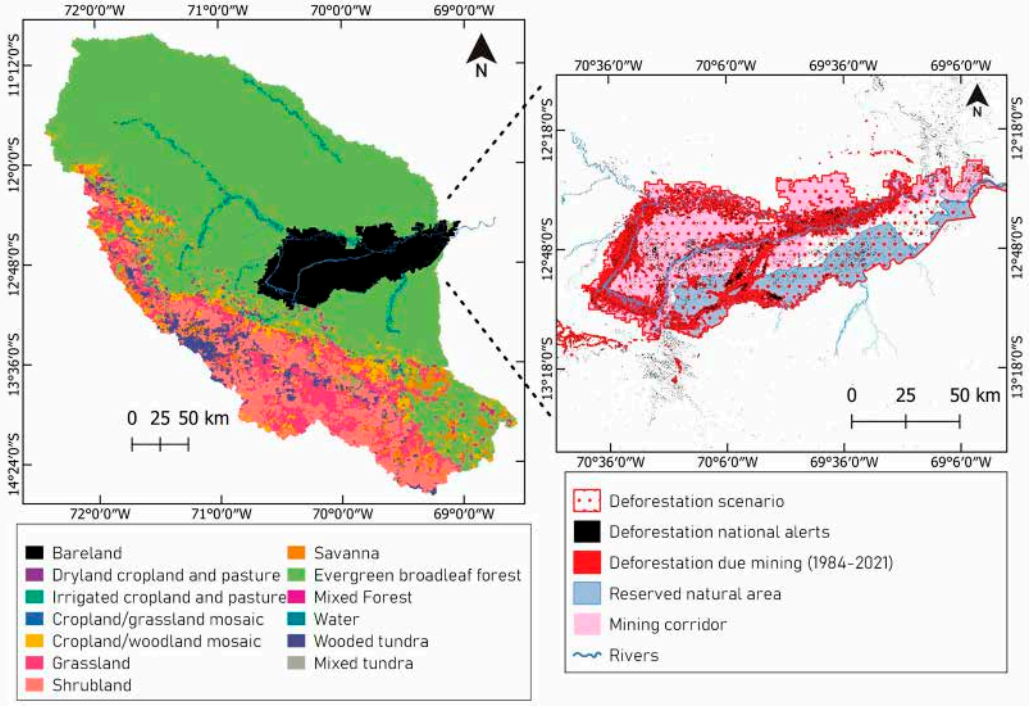

Figure 4. Land use map of the deforestation scenario. Source: Land use map: Global Land Cover Characterization (GLCC)—USGS. Deforestation national alerts: http://geobosques.minam.gob.pe (accessed on 20 March 2023) [49].

The replacement of the land cover classification, transitioning from evergreen broadleaf forest (FOEB) to bare land (BARR) to symbolize deforestation, has been previously employed in other studies. For example, in the Brazilian Amazon, researchers evaluated SWAT model outputs by substituting land cover maps with those calculated by Soares-Filho et al. [50] using the SimAmazonia model. These scenarios, referred to as the "Business as Usual" (BAU_2050) and the "Governance" (GOV_2050), were successfully implemented for the Iriri River Basin and the Upper Crepori River Basin (UCRB). These papers collectively suggest that land use change in the Amazon Basin can have significant impacts on hydrology [16,51].

To evaluate the potential impact of future deforestation on hydrologic variables, we have proposed a future deforestation scenario. This scenario is shown in Figure 4 and encompasses the highest density of deforestation alerts developed by MINAM (shown in black), deforestation resulting from mining activities (depicted in red) calculated by Caballero et al. [11], and the entire mining corridor (areas designated for mining activities). The boundaries of this scenario are demarcated by the lower edge of the buffer zone of the National Tambopata Reserve (highlighted in blue). This demarcation corresponds to 23 subbasins within the study area, covering an area of 8109 km^2 (equivalent to 9% of the total study area). Within this scenario, the land use has been transformed from FOEB to BARR.

3. Results

3.1. Correlation between Streamflows Generated by CHIRPS, TRMM, and PISCO Precipitation Datasets and In Situ Data

It is notable that the SWAT model was successful in simulating the seasonal trend of the dry and wet seasons but did not capture the maximum and minimum flows well (NS = 0.34/−0.86/0.2, PBIAS= 1.3/34.7/30.3%, and RSR = 0.81/1.37/0.9 using CHIRPS, TRMM, and PISCO, respectively). Subsequently, the decision was made to employ the CHIRPS dataset as the precipitation input for the SWAT model, given its greater perfor-

mance in terms of both the correlation coefficient (NSE) and PBIAS compared to the other datasets (as depicted in Figure 5).

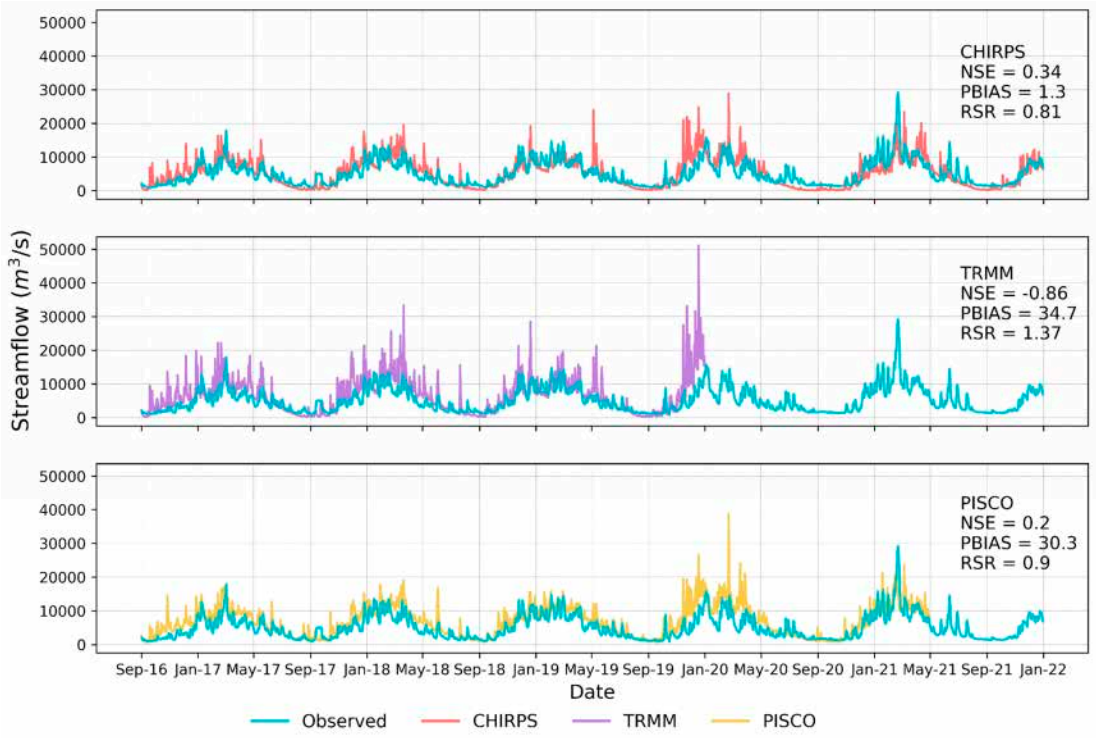

Figure 5. Time series of streamflows generated by SWAT model using CHIRPS, TRMM, and PISCO precipitation datasets and in situ data (Amaru Mayu station).

3.2. Model Performance, Calibration, and Uncertainty Analysis

The period of simulation covers four decades, from 1985 to 2021. Figure 6 shows the comparison between observed and simulated streamflows in the first run on a daily and monthly scale for the period 2016–2022. The data for the entire simulation period can be found in Appendix A.

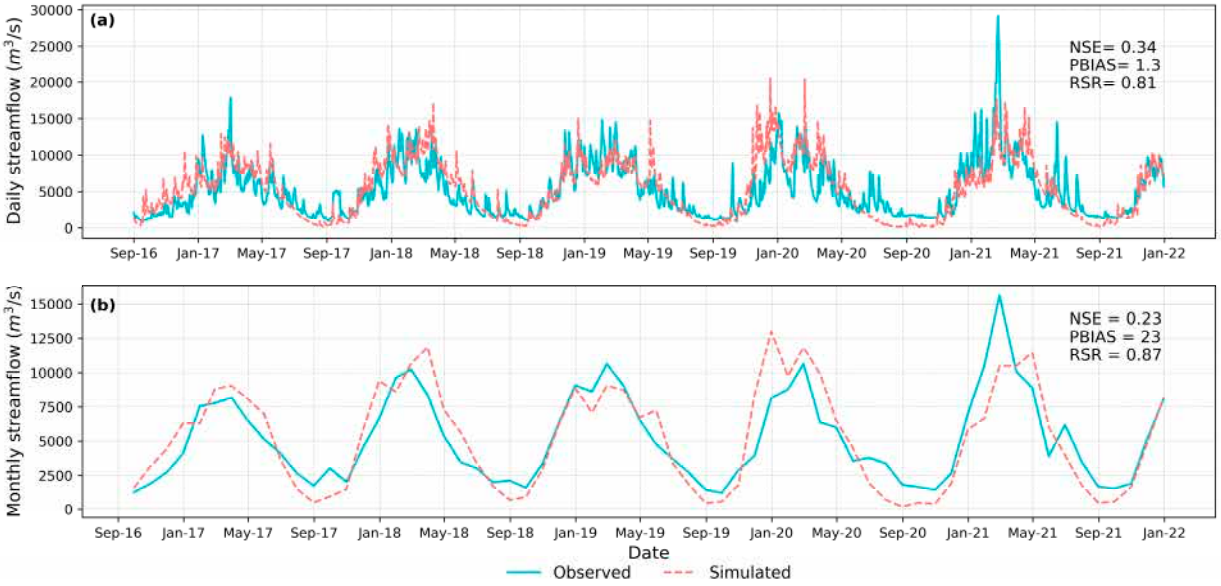

Figure 6. (**a**) Daily and (**b**) monthly time series of observed and simulated streamflow in the first model run forced using CHIRPS rainfall.

To improve the simulation, an automatic calibration was performed in the SWAT-Calibration Uncertainty Program (CUP) software, version 5.1.6.2. The Sequential Uncertainty Fitting (SUFI-2) algorithm was applied with the Nash–Sutcliffe coefficient of efficiency (NS) as the objective function [52]. One of the first steps, and an important step in automatic calibration, is identifying the parameters to optimize [53]. The parameters chosen are shown in Table 3 and were selected on the basis of the following analysis.

Table 3. Parameters included in the sensitivity analysis.

Description	Parameter	Default Value	Calibrated Range	Fitted Value
Curve number for moisture condition II.	CN2.mgt_FOEB [1]	72	0–98	46.2
	CN2.mgt_GRAS [1]	81	0–98	52.1
	CN2.mgt_SHRB [1]	76	0–98	48.8
Baseflow alpha factor (1/days).	ALPHA_BF.gw	0.048	0–1	1
Threshold depth of water in the shallow aquifer required for return flow to occur (mm H_2O).	GWQMN.gw	1000	0–5000	2009.1
Groundwater "revap" coefficient.	GWREVAP.gw	0.02	0.02–0.2	0.08
Threshold depth of water in the shallow aquifer for "revap" or percolation to the deep aquifer to occur (mm H_2O).	REVAPMN.gw	750	0–500	322
Groundwater delay time (days).	GW_DELAY.gw	31	30–450	60.26
Effective hydraulic conductivity in main channel alluvium (mm/h).	CH_K2.rte	0	0–250	51.4
Manning's "*n*" value for the main channel.	CH_N2.rte	0.014	0.01–0.3	0.06
Soil evaporation compensation factor.	ESCO.hru	1	0.01–1	0.98
Plant uptake compensation factor.	EPCO.hru	0.95	0.01–1	1
Saturated hydraulic conductivity (mm/h)	SOL_K.sol_FOEB [1]	8.93	0–2000	9.4
	SOL_K.sol_GRAS [1]	24.83	0–2000	26.14
	SOL_K.sol_SHRB [1]	37.59	0–2000	39.6

[1] FOEB, GRAS, and SHRB correspond to the land covers' evergreen broadleaf forest, grassland, and shrubland, respectively.

Figure 6 shows that the simulated streamflow during the dry season is too low against the observed flow; this may be related to groundwater water parameters such as GWQMN.gw, GW_REVAP.gw, and REVAMPM.gw [54]. The following two groundwater parameters, GW_DELAY.gw and ALPHA_BF.gw, were chosen because some studies of the Brazilian Amazon have reported them as sensitive parameters [15,16,51,55]. The ALPHA_BF factor is a constant, indicating the response of groundwater flow to any change in recharge (1/day). Since there are no previous studies on MDD reporting groundwater parameter values, the full ranges for these values were used.

Parameters related to the physical characteristics of the main channel were chosen to be calibrated since these parameters affect the flow of water and transport of sediment in the channel network of the watershed [14]. The effective hydraulic conductivity (CH_K2.rte) depends on riverbed materials, with a range of 25–76 mm/h used in the calibration corresponding to sand and gravel mixture with low silt–clay content. Manning's "*n*" coefficient for the main channel (CH_N2.rte) was also calibrated in a meaningful range.

After the sensitivity analysis achieved in SWAT-CUP, five parameters were identified as significantly sensitive (p-value < 0.05), including CH_N2.rte, CN2.mgt, GW_DELAY.gw, GWQMN.gw, and EPCO.hru. Due to limited data availability regarding these parameters

in the MDD Basin, the ranges of values were established during the calibration process, ensuring that they fall within physically meaningful limits [14]. The graphical representation contrasting observed and simulated streamflow during the calibration period (2016–2020) is depicted in Figure 7.

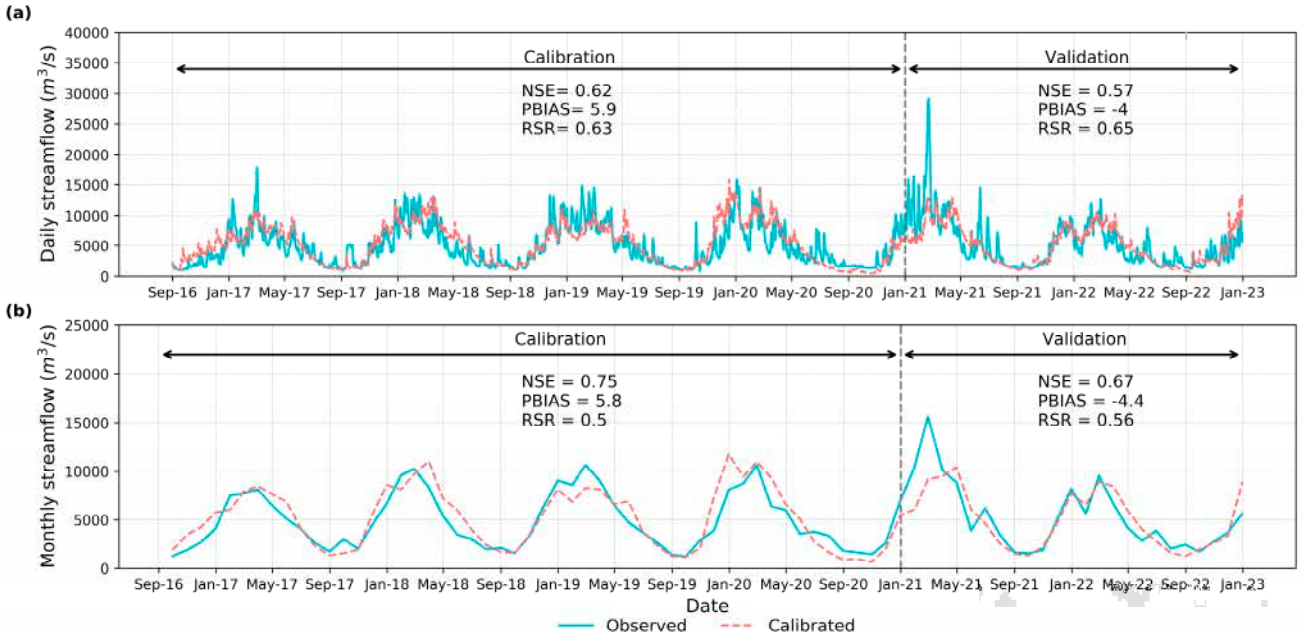

Figure 7. (**a**) Daily and (**b**) monthly time series of observed and calibrated streamflow in the hydrological station Amaru Mayu, after the calibration process.

In a daily time step simulation, we obtained an NS = 0.62/0.57, PBIAS = 5.9/−4, and RSR = 0.63/0.65 for the calibration and validation periods, respectively. In a monthly time step simulation, values of NS = 0.75/0.67, PBIAS = 5.8/−4.4, and RSR = 0.5/0.56 were obtained for the calibration and validation periods, respectively.

These values indicate "Good" (daily) and "Very good" (monthly) levels of consistency in comparison with the criteria presented in Table 2 [45]. Owing to the calibration step, the model performances improved by 0.28 and 0.8 in terms of NSE.

3.3. Hydrological Basin Response Corresponding to the Deforestation Scenario Simulation

The simulation was conducted by replacing the original baseline land use map with the deforestation scenario land use map (depicted in Figure 4) within the calibrated model. This was carried out to analyze the impact of LULC changes on the hydrology of the study area. This modification was implemented while maintaining consistency with the other SWAT inputs, including the DEM, soil map, and climate data. Within the deforestation scenario, a targeted change was introduced, involving the replacement of 12% of the total area covered by evergreen broadleaf forest (FOEB) with bare land (BARR).

3.3.1. Average Monthly Means

Figure 8 shows the monthly values for the water balance components, including surface runoff, lateral flow, groundwater flow, water yield, evapotranspiration, and streamflow, in both the baseline and deforestation scenarios. The surface runoff values exhibit their peak from October to April (during the rainy season), while they are at their lowest from May to September (referred to as the dry season).

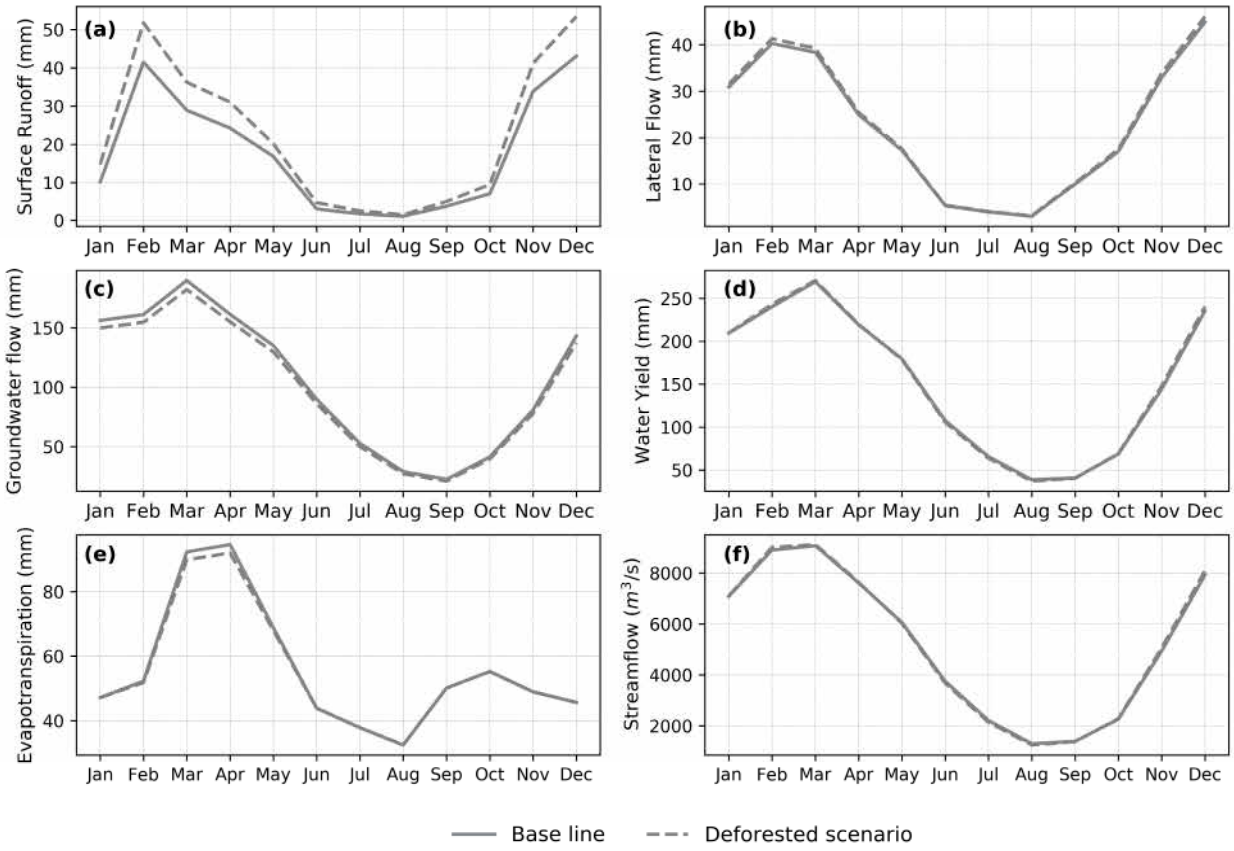

Figure 8. Monthly average simulated (**a**) surface runoff (mm), (**b**) lateral flow (mm), (**c**) groundwater flow (mm), (**d**) water yield (mm), (**e**) evapotranspiration (mm), and (**f**) streamflow ($m^3 \cdot s^{-1}$).

The monthly impacts of LULC variations from the baseline to deforested scenario have been noted on the surface runoff. Conversely, the influence of LULC variations on the monthly values of lateral flow, groundwater, water yield, and evapotranspiration is comparatively minor. Table 4 displays the percentage changes.

Table 4. Percentage changes of monthly average water balance components, including surface runoff (SURQ), lateral flow (LATQ), water yield (WY), evapotranspiration (ET), and groundwater flow (GWQ), under both baseline and deforested scenarios.

Hydrological Component	Jan	Feb	Mar	Apr	May	Jun	Jul	Aug	Sep	Oct	Nov	Dec
	Percentage Change%											
SURQ	45.7	24.7	25.2	27.8	19.4	54.5	47	35.2	34.4	35.1	21.6	23.9
LATQ	2.1	2.6	2.3	2.0	1.7	1.7	2.6	3.4	3.0	2.8	2.9	2.6
WY	0.1	1.3	0.5	0.3	−0.6	−1.9	−3.0	−4.2	−0.8	0.8	2.5	2.1
ET	−0.04	−0.9	−2.7	−2.8	−1.3	0.1	0.1	0.1	0	−0.1	−0.04	−0.04
GWQ	−4.1	−4.0	−4.0	−3.9	−3.9	−4.3	−5.3	−6.6	−6.6	−4.3	−3.8	−4.0

Surface runoff indicates a monthly average increase of 33%, with its most significant increases taking place during the dry season (May to September) at a rate of 38%, while the least notable increments occurring during the wet season (October to April) at 29%. Lateral flow has experienced a slight increase of 3%, primarily during the period from July to December. Notably, water yield displays distinct variations between seasons, with a 1% increase during the dry season and a 2% decline during the wet season. An evident decrease in evapotranspiration is observed, especially during the period from February to

May, with a reduction of 2%. Likewise, there has been an average monthly decrease of 5% in groundwater flow.

3.3.2. Average Annual Means

Table 5 depicts the effects of land cover change on the MDD Basin. The findings demonstrate that, under both scenarios, there is an increase in the average annual surface runoff, lateral flow, and water yield, by 26.2%, 2.4%, and 0.4%, respectively, between both scenarios. Conversely, groundwater flow, percolation, and evapotranspiration decrease by 4.2%, 3.8%, and 1%, respectively. These changes were attributed to the conversion of forest to bare land in the deforested scenario, as other climate and soil components were kept constant. Figure 9 provides a summary of the changes in annual water balance components.

Table 5. Percentage changes in the annual average values of the water balance components, including surface runoff (SURQ), lateral flow (LATQ), groundwater (GWQ), water yield (WY), and evapotranspiration (ET), under both baseline and deforested scenarios.

Scenario	SURQ	LATQ	GWQ	WY	PERC	ET
Baseline	215.6	269.1	1337.1	1821.5	1503.8	669.8
Deforested scenario	272.1	275.6	1281.5	1829	1447.2	663.3
% change	26.2	2.4	−4.2	0.4	−3.8	−1

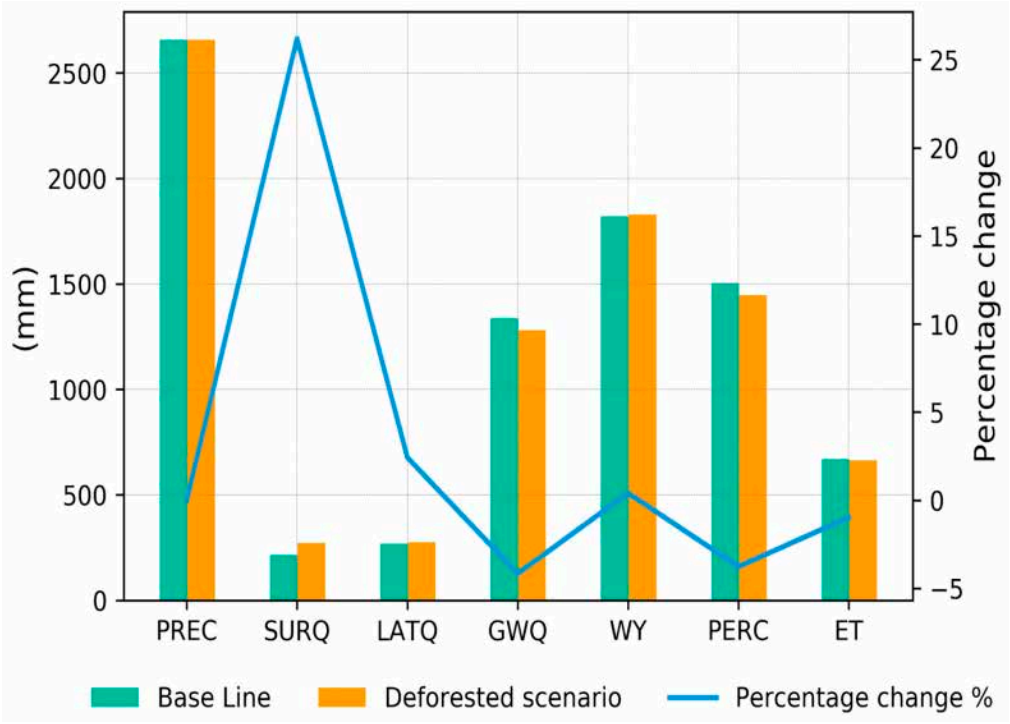

Figure 9. Annual average amounts and percentage changes in the water balance components in both baseline and deforested scenarios.

3.3.3. Average Annual Means at Subbasin Scale

Figure 10 displays the alterations in average annual surface runoff at a subbasin scale. The main changes exhibit consistency within the region where the land cover change was implemented for the deforested scenario. This deforested area had an impact on a total of 26 subbasins, which observed an average annual surge of 164% in surface runoff. Among these, the subbasin of the Inambari River demonstrated a notable increase of 187%.

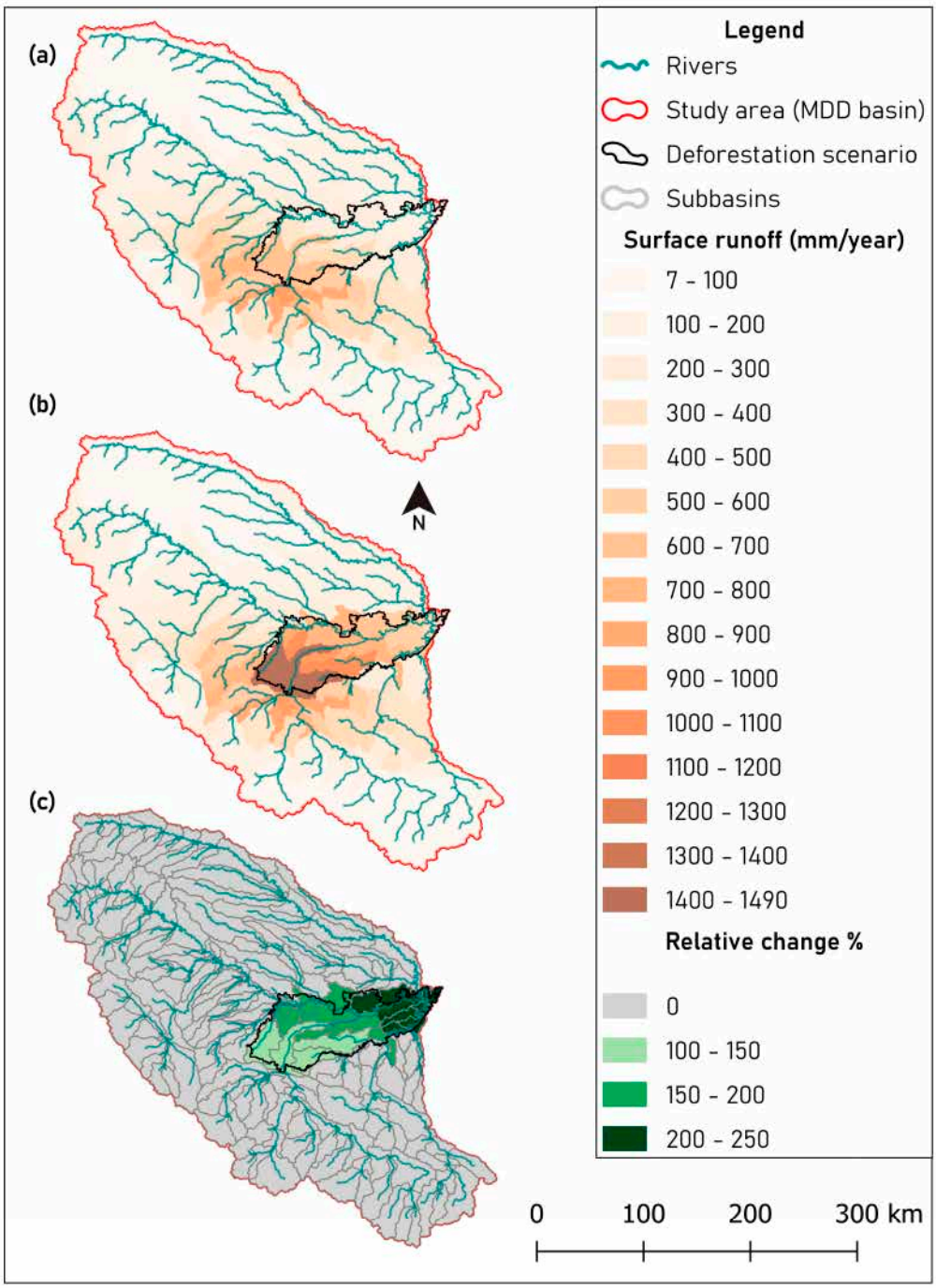

Figure 10. Annual average surface runoff at the subbasin scale in (**a**) baseline and (**b**) deforested scenarios. (**c**) Relative percentage change between both scenarios.

Figure 11 shows the changes in average annual evapotranspiration at the subbasin scale. As observed with surface runoff trends, this decline is particularly pronounced within the deforested region. Among the subbasins, one that stands out for its considerable impact is the lower segment of the Inambari River subbasin, where there was a notable 8% reduction in evapotranspiration. Moreover, it is noteworthy that, on average, the subbasins that encountered alterations experienced a decrease of 7% in their annual average evapotranspiration.

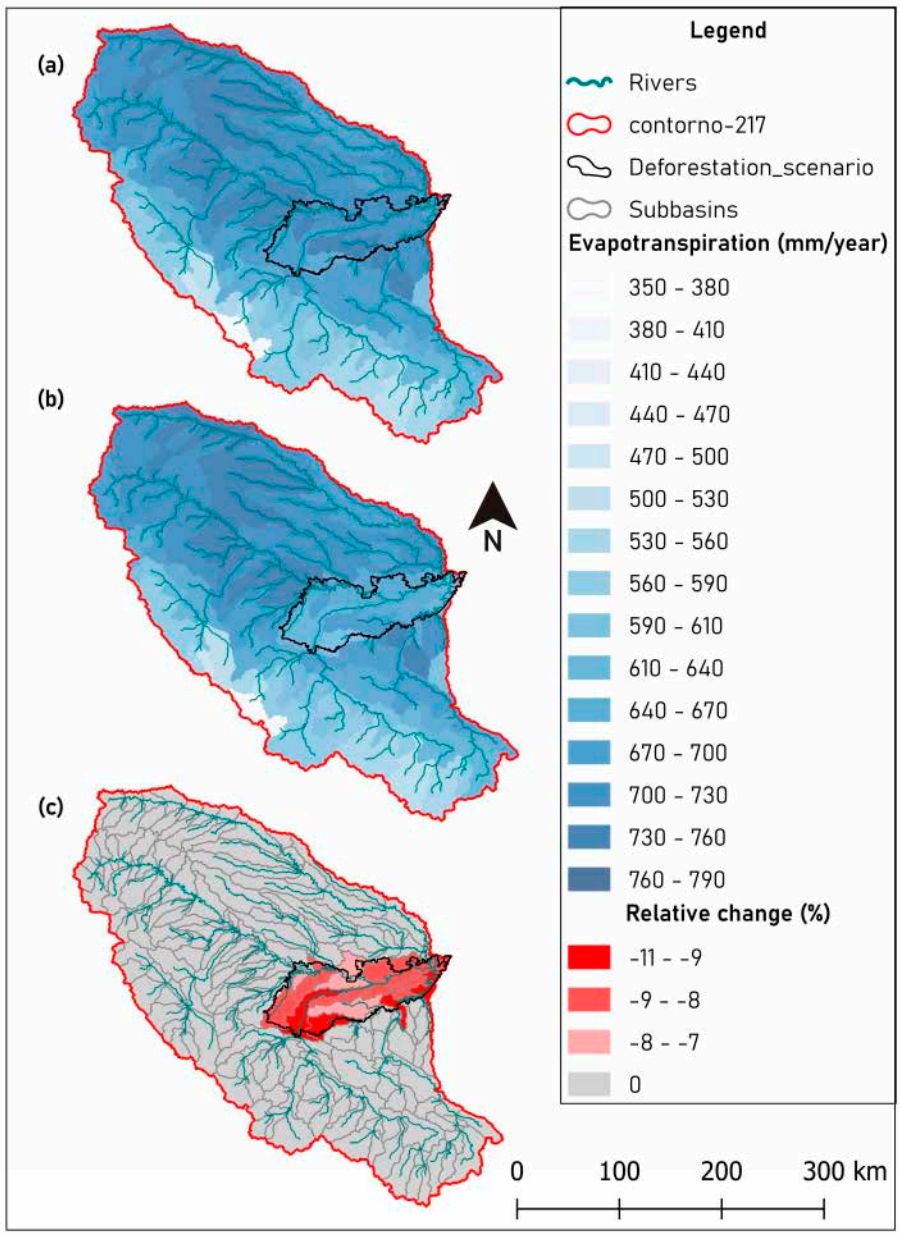

Figure 11. Annual average evapotranspiration at the subbasin scale in (**a**) baseline and (**b**) deforested scenarios. (**c**) Relative percentage change between both scenarios.

4. Discussion

Deforestation within the MDD Basin persists as a threat that impacts the environment from multiple perspectives. Unfortunately, the watershed still lacks comprehensive hydrological information. To address this gap, hydrological modeling was achieved to investigate how water balance components react to increasing deforestation levels in the MDD Basin.

This study focuses on LULC changes, specifically the deforestation scenario, which involves replacing 12% of evergreen broadleaf forest, which covers 9% of the study area, with bare land. The impact of these changes has been observed in terms of surface runoff, water yield, groundwater flow, and lateral flow. Notably, surface runoff registers the most significant increase, exceeding other components, both on a monthly and an annual scale. This change can be attributed to the greater availability of water in deforested areas, leading to increased infiltration and surface runoff processes, while simultaneously reducing the interception process.

Surface runoff has a monthly average increase of 33% over the basin; this increment is more noticeable during the dry season (38%) than the wet season (29%). This hydrological component remained the biggest increase, by 26%, in the annual average. At the subbasin scale, there is a consistent increment in surface runoff within the deforested area, impacting a total of 26 subbasins. This influence is particularly notable on one of the primary tributaries of the Madre de Dios River, the Inambari River, in which basin the average increase reaches a substantial 187% annually. Such change is likely to cause unprecedented floods that are likely to have strong human and economic impacts [56], especially when cities expand over susceptible to flooding areas [57]. The increase of surface runoff consequently increases the monthly streamflow by 12% at the outlet of the basin. Increases in streamflow can lead to flooding and extreme inundation events, as has already occurred in the MDD region.

The effects of the loss of forest is also evident in the reduction of the monthly average evapotranspiration by 2% during the period from February to May. When considering the spatial scale, it is noticeable that the change is uniformly distributed over the deforested area, with the subbasins that encountered alterations experiencing a decrease of 7% in their annual average evapotranspiration.

The impact of LULC alteration on soil water content and lateral flow reveals smaller increments, both on a monthly and an annual scale. In contrast, groundwater experiences a consistent decline, which is evident across both monthly observations and yearly trends. These outcomes align with anticipated patterns when forested regions transition to barren soil or alternative forms of land cover, as reported in prior studies [58]. It is worth emphasizing that subbasins within the deforested area exhibit substantial localized changes, which might not be fully captured in the average values across the broader study area. This demonstrates that forested land possesses the highest capacity for water yield and evaporation, while bare land exhibits the lowest evaporation and the highest surface runoff production capacity. These findings align with conclusions drawn from previous studies [13,16,58–60].

Despite meeting the criteria for good and very good model performance, the SWAT model exhibited a tendency to underestimate low flows during the dry seasons, as well as peak flows during the high season. This outcome is considered acceptable due to the limitations of the observed data available for the calibration and validation steps, covering only seven years, and the fact that the SWAT model was calibrated with a single streamflow station. Another source of uncertainty in the simulations arises from the initial input data, including precipitation and temperature data, which inherently carries its own degree of uncertainty as it relies on satellite-based products. Nevertheless, the correction of these uncertainties for the Peruvian Amazonian Basin falls beyond the scope of the present study and should be explored in future research.

5. Conclusions

This study implemented the hydrological model SWAT to assess the impact of deforestation in the hydrology of the MDD Basin. The parameters related to groundwater were shown to be the most sensitive in the calibration process. A good rating was obtained for the performance of the monthly model (NS = 0.75 and PBIAS = 0.67).

Results showed that the deforested scenario alters the hydrology of the MDD Basin. The observed alterations exhibit a more pronounced contrast when examined on a monthly basis rather than an annual one. Notably, during the dry season, there is a substantial 38% increase in surface runoff, while in the wet season, there is a marginal 2% reduction in evapotranspiration. Conversely, variables such as lateral flow, groundwater flow, and water yield manifest negligible adjustments, all falling below the 3% threshold, both in annual and monthly assessments. On a spatial scale, the most notable effects are evident in surface runoff and evapotranspiration variables, particularly within the deforestation scenario, impacting a total of 26 subbasins. Among these, the Inambari River Basin stands out as the most severely affected, witnessing a substantial annual increase of 187% in runoff and a

concurrent annual decrease of 7% in evapotranspiration, corroborating the hypothesis that the Inambari River is one of the most important tributaries of the Madre de Dios River.

The documented rise in surface runoff, as established in this research, could potentially impede future reforestation initiatives owing to heightened soil erosion rates. Moreover, increased surface runoff will cause a substantial load of sediments, potentially polluted, resulting in the degradation of river ecosystems and human health. Furthermore, our results underscore the significance of the implementation of effective conservation strategies within the MDD Basin for safeguarding the Amazonian forests.

Future research should encompass the analysis of additional factors like predictions of future deforestation, utilizing remote sensing products for a more comprehensive understanding of the dynamics of land cover within the basin. Furthermore, it should be supplemented by the collection of data on soil physical and mechanical parameters, to improve model representation issues. To enhance the outcomes of this study, it is imperative to enhance the hydroclimatological measurement network. This enhancement should involve a comprehensive assessment of sediment measurements and the installation of hydrological stations in main tributaries to facilitate the implementation of complex calibration strategies of these crucial variables, potentially influencing initiatives aimed at conserving hydrobiological ecosystems.

Author Contributions: Methodology, P.R.; Writing—original draft, K.P.; Writing—review & editing, L.B. and F.F.; Supervision, C.M. and W.L.-C. All authors have read and agreed to the published version of the manuscript.

Funding: This research received no external funding.

Data Availability Statement: The data presented in this study are available on request from the corresponding author.

Acknowledgments: We thank the authors of the "Impacts of alluvial mining in the Madre de Dios watershed: physical effects and mitigation planning" project (PEER 8-235) for their collaboration and technical assistance. The "River Mining" project was implemented in the period 2020–2022 by the Center for Water Research and Technology (CITA) of the Technological and Engineering University (UTEC). We also thank anonymous reviewers for their feedback and comments.

Conflicts of Interest: The authors declare no conflict of interest.

Appendix A. Streamflow Simulation in the MDD Basin (Amaru Mayu Station)

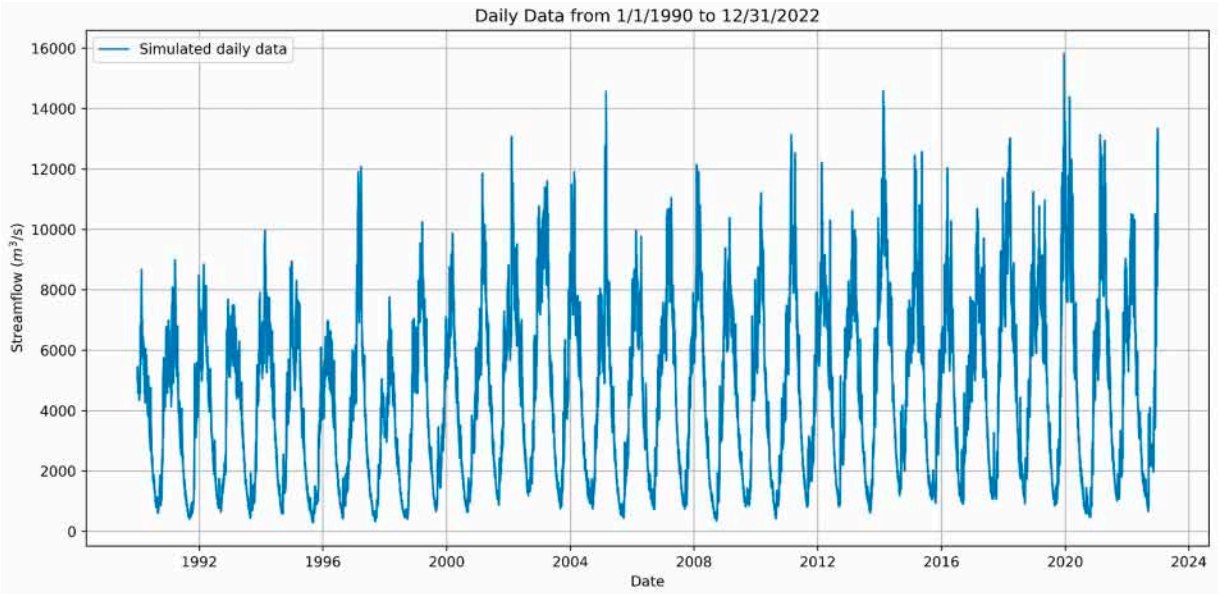

Figure A1. Daily streamflow simulated by the calibrated model at the outlet of the MDD Basin (Amaru Mayu station) for the period 1990–2022.

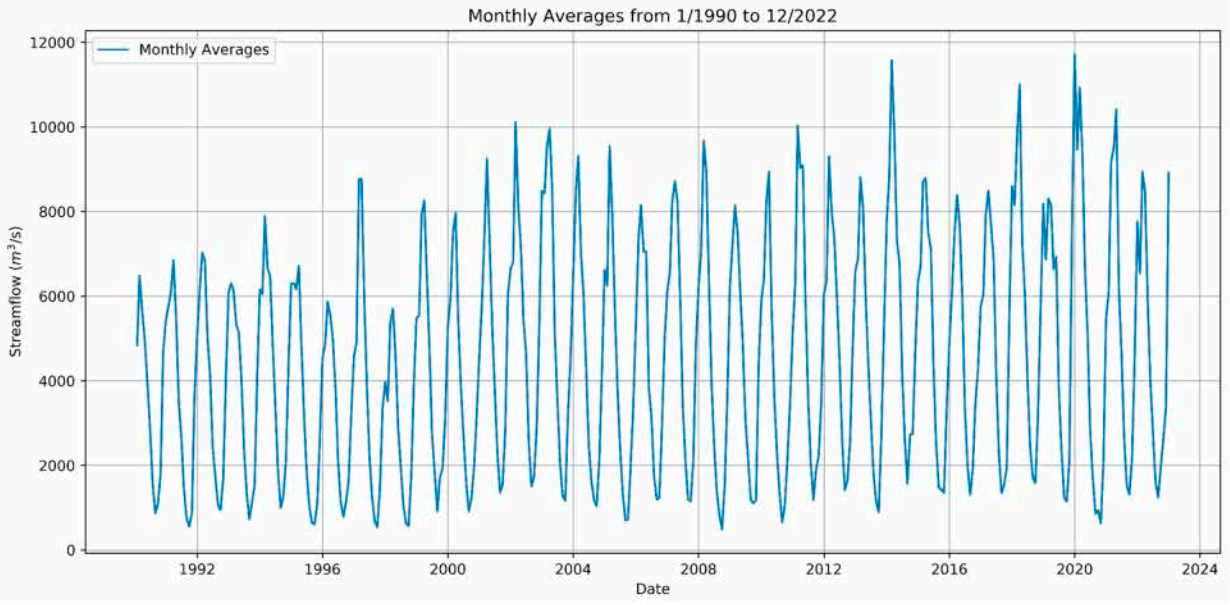

Figure A2. Monthly streamflow simulated by the calibrated model at the outlet of the MDD Basin (Amaru Mayu station) for the period 1990–2022.

References

1. Ceballos, G.; Ehrlich, P.R. Global mammal distributions, biodiversity hotspots, and conservation. *Proc. Natl. Acad. Sci. USA* **2006**, *103*, 19374–19379. [CrossRef] [PubMed]
2. Markham, K.E. Sangermano, Florencia. Evaluating wildlife vulnerability to mercury pollution from artisanal and small-scale gold mining in Madre de Dios, Peru. *Trop. Conserv. Sci.* **2018**, *11*, 1940082918794320. [CrossRef]
3. Myers, N.; Mittermeier, R.A.; Mittermeier, C.G.; Da Fonseca, G.A.; Kent, J. Biodiversity hotspots for conservation priorities. *Nature* **2000**, *403*, 853–858. [CrossRef] [PubMed]
4. Asner, G.P.; Knapp, D.E.; Martin, R.E.; Tupayachi, R.; Anderson, C.B.; Mascaro, J.; Sinca, F.; Chadwick, K.D.; Higgins, M.; Farfan, W.; et al. Targeted carbon conservation at national scales with high-resolution monitoring. *Proc. Natl. Acad. Sci. USA* **2014**, *111*, E5016–E5022. [CrossRef] [PubMed]
5. Asner, G.P.; Tupayachi, R. Accelerated losses of protected forests from gold mining in the Peruvian Amazon. *Environ. Res. Lett.* **2017**, *12*, 094004. [CrossRef]
6. Telmer, K.H.; Veiga, M.M. World emissions of mercury from artisanal and small scale gold mining. In *Mercury Fate and Transport in the Global Atmosphere: Emissions, Measurements and Models*; Springer US: Boston, MA, USA, 2009; pp. 131–172.
7. Ashe, K. Elevated mercury concentrations in humans of Madre de Dios, Peru. *PLoS ONE* **2012**, *7*, e33305. [CrossRef]
8. Martinez, G.; McCord, S.A.; Driscoll, C.T.; Todorova, S.; Wu, S.; Araújo, J.F.; Vega, C.M.; Fernandez, L.E. Mercury contamination in riverine sediments and fish associated with artisanal and small-scale gold mining in Madre de Dios, Peru. *Int. J. Environ. Res. Public Health* **2018**, *15*, 1584. [CrossRef]
9. Gonzalez, D.J.; Arain, A.; Fernandez, L.E. Mercury exposure, risk factors, and perceptions among women of childbearing age in an artisanal gold mining region of the Peruvian Amazon. *Environ. Res.* **2019**, *179*, 108786. [CrossRef]
10. Gerson, J.; Topp, S.; Vega, C.M.; Gardner, J.; Yang, X.; Fernández, L.E.; Bernhardt, E.; Pavelsky, T. *Artisanal Gold Mining Ponds Amplify Mercury Risk in the Peruvian Amazon (Research Brief CINCIA #7)*; Centro de Innovación Científica Amazónica: Puerto Maldonado, Peru, 2021.
11. Caballero, J.; Messinger, M.; Román-Dañobeytia, F.; Ascorra, C.; Fernandez, L.E.; Silman, M. Deforestation and forest degradation due to gold mining in the Peruvian Amazon: A 34-year perspective. *Remote Sens.* **2018**, *10*, 1903. [CrossRef]
12. Householder, J.E.; Janovec, J.P.; Tobler, M.W.; Page, S.; Lähteenoja, O. Peatlands of the Madre de Dios River of Peru: Distribution, geomorphology, and habitat diversity. *Wetlands* **2012**, *32*, 359–368. [CrossRef]
13. Liang, J.; Wu, K.; Li, Y.; Wei, Z.; Zhuo, P.; Yan, Q.; Luo, X. Impacts of large-scale rare earth mining on surface runoff, groundwater, and evapotranspiration: A case study using SWAT for the Taojiang River Basin in Southern China. *Mine Water Environ.* **2019**, *38*, 268–280. [CrossRef]
14. Arnold, J.G.; Kiniry, J.R.; Srinivasan, R.; Williams, J.R.; Haney, E.B.; Neitsch, S.L. SWAT 2012 Input/Output Documentation. Texas Water Resources Institute 2013. Available online: https://hdl.handle.net/1969.1/149194 (accessed on 5 December 2023).
15. De Oliveira Serrão, E.A.; Silva, M.T.; Ferreira, T.R.; de Ataide LC, P.; dos Santos, C.A.; de Lima AM, M.; Gomes DJ, C. Impacts of land use and land cover changes on hydrological processes and sediment yield determined using the SWAT model. *Int. J. Sediment Res.* **2022**, *37*, 54–69. [CrossRef]

16. Abe, C.A.; Lobo, F.D.L.; Dibike, Y.B.; Costa, M.P.D.F.; Dos Santos, V.; Novo, E.M.L. Modeling the effects of historical and future land cover changes on the hydrology of an Amazonian basin. *Water* **2018**, *10*, 932. [CrossRef]
17. Baker, T.J.; Miller, S.N. Using the Soil and Water Assessment Tool (SWAT) to assess land use impact on water resources in an East African watershed. *J. Hydrol.* **2013**, *486*, 100–111. [CrossRef]
18. Fassoni-Andrade, A.C.; Fleischmann, A.S.; Papa, F.; de Paiva, R.C.D.; Wongchuig, S.; Melack, J.M.; Moreira, A.A.; Paris, A.; Ruhoff, A.; Barbosa, C.; et al. Amazon hydrology from space: Scientific advances and future challenges. *Rev. Geophys.* **2021**, *59*, e2020RG000728. [CrossRef]
19. Tuo, Y.; Duan, Z.; Disse, M.; Chiogna, G. Evaluation of precipitation input for SWAT modeling in Alpine catchment: A case study in the Adige river basin (Italy). *Sci. Total Environ.* **2016**, *573*, 66–82. [CrossRef]
20. Huffman, G.J.; Bolvin, D.T.; Nelkin, E.J.; Wolff, D.B.; Adler, R.F.; Gu, G.; Hong, Y.; Bowman, K.P.; Stocker, E.F. The TRMM multisatellite precipitation analysis (TMPA): Quasi-global, multiyear, combined-sensor precipitation estimates at fine scales. *J. Hydrometeorol.* **2007**, *8*, 38–55. [CrossRef]
21. Schwaller, M.R.; Morris, K.R. A Ground Validation Network for the Global Precipitation Measurement Mission. *J. Atmos. Ocean. Technol.* **2011**, *28*, 301–319. [CrossRef]
22. Funk, C.; Verdin, A.; Michaelsen, J.; Peterson, P.; Pedreros, D.; Husak, G. A global satellite-assisted precipitation climatology. *Earth Syst. Sci. Data* **2015**, *7*, 275–287. [CrossRef]
23. de Paiva, R.C.D.; Buarque, D.C.; Collischonn, W.; Bonnet, M.-P.; Frappart, F.; Calmant, S.; Bulhões Mendes, C.A. Large-scale hydrologic and hydrodynamic modeling of the Amazon River basin. *Water Resour. Res.* **2013**, *49*, 1226–1243. [CrossRef]
24. Zubieta, R.; Getirana, A.; Espinoza, J.C.; Lavado-Casimiro, W.; Aragon, L. Hydrological modeling of the Peruvian–Ecuadorian Amazon Basin using GPM-IMERG satellite-based precipitation dataset. *Hydrol. Earth Syst. Sci.* **2017**, *21*, 3543–3555. [CrossRef] [PubMed]
25. Balcázar, L.; Bâ, K.M.; Díaz-Delgado, C.; Quentin, E.; Minga-León, S. Modelado de caudales diarios en una cuenca del sur del Ecuador con precipitación y temperatura estimadas por satélite. *Agrociencia* **2019**, *53*, 465–486.
26. CPC Global Unified Temperature Data Provided by the NOAA PSL, Boulder, Colorado, USA. Available online: https://psl.noaa.gov (accessed on 29 March 2023).
27. Diringer, S.E.; Berky, A.J.; Marani, M.; Ortiz, E.J.; Karatum, O.; Plata, D.L.; Pan, W.K.; Hsu-Kim, H. Deforestation due to artisanal and small-scale gold mining exacerbates soil and mercury mobilization in Madre de Dios, Peru. *Environ. Sci. Technol.* **2019**, *54*, 286–296. [CrossRef] [PubMed]
28. Swenson, J.J.; Carter, C.E.; Domec, J.C.; Delgado, C.I. Gold mining in the Peruvian Amazon: Global prices, deforestation, and mercury imports. *PLoS ONE* **2011**, *6*, e18875. [CrossRef] [PubMed]
29. Callan, N.; De la Cruz, A.; Guerrero, L.; Santillan, B.; Langendoen, E.; Moreno, M. Bedform Dynamics in the Mining-Impacted Madre de Dios River, Peruvian Amazon. Research Brief. River Mining Project (PEER 8-235). 2023. Available online: https://cincia.wfu.edu/category/publicaciones/ (accessed on 5 December 2023).
30. Castro, A.; Dávila, C.; Laura, W.; Cubas Saucedo, F.; Ávalos, G.; López, C.; Villena, D.; Valdez, M.; Urbiola, J.; Trebejo, I.; et al. Climas del Perú: Mapa de Clasificación Climática Nacional. Servicio Nacional de Meteorología e Hidrología del Perú (SENAMHI) 2021. Available online: https://pesquisa.bvsalud.org/portal/resource/pt/biblio-1292421 (accessed on 10 December 2021).
31. Finer, M.; Ariñez, A.; Mamani, N. Deforestación por Minería de Oro en la Amazonía 2023. MAAP: 178. Available online: https://maaproject.org/2023/mineria-amazonia/ (accessed on 3 March 2023).
32. Hansen, M.C.; Potapov, P.V.; Moore, R.; Hancher, M.; Turubanova, S.A.; Tyukavina, A.; Thau, D.; Stehman, S.V.; Goetz, S.J.; Loveland, T.R.; et al. High-resolution global maps of 21-st-century forest cover change. *Science* **2013**, *342*, 850–853. Available online: https://www.globalforestwatch.org/map/ (accessed on 24 July 2023). [CrossRef] [PubMed]
33. Infografías de los Datos de la Cobertura y Pérdida de Bosques al 2018. Programa Nacional de Conservación de Bosque para la Mitigación del Cambio Climático 2019. Available online: https://sinia.minam.gob.pe/documentos/infografias-datos-cobertura-perdida-bosques-2018 (accessed on 31 January 2023).
34. Aybar, C.; Fernández, C.; Huerta, A.; Lavado, W.; Vega, F.; Felipe-Obando, O. Construction of a high-resolution gridded rainfall dataset for Peru from 1981 to the present day. *Hydrol. Sci. J.* **2020**, *65*, 770–785. [CrossRef]
35. Bennett, N.D.; Croke, B.F.; Guariso, G.; Guillaume, J.H.; Hamilton, S.H.; Jakeman, A.J.; Andreassian, V. Characterising performance of environmental models. *Environ. Model. Softw.* **2013**, *40*, 1–20. [CrossRef]
36. Observatorio del Agua. Sistema Nacional de Información de los Recursos Hídricos. Autoridad Nacional del Agua. Available online: https://snirh.ana.gob.pe/ObservatorioSNIRH/ (accessed on 12 August 2022).
37. Farr, T.G.; Rosen, P.A.; Caro, E.; Crippen, R.; Duren, R.; Hensley, S.; Kobrick, M.; Paller, M.; Rodriguez, E.; Roth, L.; et al. The shuttle radar topography mission. *Rev. Geo-Phys.* **2007**, *45*, RG2004. [CrossRef]
38. FAO. *Soil Map of the World*; United Nations Educational, Scientific, and Cultural Organization; UNESCO: Paris, France, 1995.
39. USGS. *Global Land Cover Characterization*; United State Geological Survey: Washington, DC, USA, 1997.
40. Arnold, J.G.; Srinivasan, R.; Muttiah, R.S.; Williams, J.R. Large area hydrologic modeling and assessment part I: Model development 1. *JAWRA J. Am. Water Resour. Assoc.* **1998**, *34*, 73–89. [CrossRef]
41. Gassman, P.W.; Reyes, M.R.; Green, C.H.; Arnold, J.G. The soil and water assessment tool: Historical development, applications, and future research directions. *Trans. ASABE* **2007**, *50*, 1211–1250. [CrossRef]

42. Neitsch, S.L.; Arnold, J.G.; Kiniry, J.R.; Williams, J.R. Soil and Water Assessment Tool Theoretical Documentation Version 2009. Texas Water Resources Institute 2011. Available online: https://swat.tamu.edu/media/99192/swat2009-theory.pdf (accessed on 10 June 2021).
43. Dile, Y.T.; Daggupati, P.; George, C.; Srinivasan, R.; Arnold, J. Introducing a new open source GIS user interface for the SWAT model. *Environ. Model. Softw.* **2016**, *85*, 129–138. [CrossRef]
44. Daggupati, P.; Pai, N.; Ale, S.; Doulgas-Mankin, K.R.; Zeckoski, R.; Jeong, J.; Parajuli, P.; Saraswat, D.; Youssef, M. A recommended calibration and validation strategies for hydrological and water quality models. *Trans. ASABE* **2015**, *58*, 1705–1719.
45. Moriasi, D.N.; Arnold, J.G.; Van Liew, M.W.; Bingner, R.L.; Harmel, R.D.; Veith, T.L. Model evaluation guidelines for systematic quantification of accuracy in watershed simulations. *Trans. ASABE* **2007**, *50*, 885–900. [CrossRef]
46. Nash, J.E.; Sutcliffe, J.V. River flow forecasting through conceptual models: Part 1. d A discussion of principles. *J. Hydrol.* **1970**, *10*, 282–290. [CrossRef]
47. Gupta, H.; Sorooshian, S.; Yapo, P. Status of automatic calibration for hydro- logic models: Comparison with multilevel expert calibration. *J. Hydrol. Eng.* **1999**, *4*, 135–143. [CrossRef]
48. Moriasi, D.N.; Pai, N.; Steiner, J.L.; Gowda, P.H.; Winchell, M.; Rathjens, H.; Starks, P.J.; Verser, J.A. SWAT-LUT: A desktop graphical user interface for updating land use in SWAT. *JAWRA J. Am. Water Resour. Assoc.* **2019**, *55*, 1102–1115. [CrossRef]
49. Vargas, C.; Montalban, J.; Leon, A.A. Early warning tropical forest loss alerts in Peru using Landsat. *Environ. Res. Commun.* **2019**, *1*, 121002. [CrossRef]
50. Soares-Filho, B.S.; Nepstad, D.C.; Curran, L.M.; Cerqueira, G.C.; Garcia, R.A.; Ramos, C.A.; Voll, E.; McDonald, A.; Lefebvre, P.; Schlesinger, P. Modelling conservation in the Amazon basin. *Nature* **2006**, *440*, 520–523. [CrossRef]
51. Dos Santos, V.; Laurent, F.; Abe, C.; Messner, F. Hydrologic response to land use change in a large basin in eastern Amazon. *Water* **2018**, *10*, 429. [CrossRef]
52. Abbaspour, K.C. *SWAT-CUP: SWAT Calibration and Uncertainty Programs—A User Manual*; Eawag: Dübendorf, Switzerland, 2015; 103p.
53. Abbaspour, K.C.; Vaghefi, S.A.; Srinivasan, R. A guideline for successful calibration and uncertainty analysis for soil and water assessment: A review of papers from the 2016 international SWAT conference. *Water* **2017**, *10*, 6. [CrossRef]
54. Abbaspour, K.C.; Rouholahnejad, E.; Vaghefi, S.A.; Srinivasan, R.; Yang, H.; Kløve, B. A continental-scale hydrology and water quality model for Europe: Calibration and uncertainty of a high-resolution large-scale SWAT model. *J. Hydrol.* **2015**, *524*, 733–752. [CrossRef]
55. Strauch, M.; Volk, M. SWAT plant growth modification for improved modeling of perennial vegetation in the tropics. *Ecol. Model.* **2013**, *269*, 98–112. [CrossRef]
56. Kreibich, H.; Van Loon, A.F.; Schröter, K.; Ward, P.J.; Mazzoleni, M.; Sairam, N.; Abeshu, G.W.; Agafonova, S.; AghaKouchak, A.; Aksoy, H.; et al. The challenge of unprecedented floods and droughts in risk management. *Nature* **2022**, *608*, 80–86. [CrossRef] [PubMed]
57. García-Rivero, A.E.; Olivera, J.; Salinas, E.; Yuli, R.A.; Bulege, W. Use of hydrogeomorphic indexes in SAGA-GIS for the characterization of flooded areas in Madre de Dios, Peru. *Int. J. Appl. Eng. Res.* **2017**, *12*, 9078–9086.
58. Abuhay, W.; Gashaw, T.; Tsegaye, L. Assessing impacts of land use/land cover changes on the hydrology of Upper Gilgel Abbay watershed using the SWAT model. *J. Agric. Food Res.* **2023**, *12*, 100535. [CrossRef]
59. Zhang, H.; Wang, B.; Liu, D.L.; Zhang, M.; Leslie, L.M.; Yu, Q. Using an improved SWAT model to simulate hydrological responses to land use change: A case study of a catchment in tropical Australia. *J. Hydrol.* **2020**, *585*, 124822. [CrossRef]
60. Gashaw, T.; Tulu, T.; Argaw, M.; Worqlul, A.W. Modeling the hydrological impacts of land use/land cover changes in the Andassa watershed, Blue Nile Basin, Ethiopia. *Sci. Total Environ.* **2018**, *619*, 1394–1408. [CrossRef]